Vol 459|11 June 2009|doi:10.1038/nature08105

LETTERS

Direct observation of a widely tunable bandgap in bilayer graphene

Yuanbo Zhang[1]*, Tsung-Ta Tang[1]*†, Caglar Girit[1], Zhao Hao[2,4], Michael C. Martin[2], Alex Zettl[1,3], Michael F. Crommie[1,3], Y. Ron Shen[1,3] & Feng Wang[1,3]

The electronic bandgap is an intrinsic property of semiconductors and insulators that largely determines their transport and optical properties. As such, it has a central role in modern device physics and technology and governs the operation of semiconductor devices such as p–n junctions, transistors, photodiodes and lasers[1]. A tunable bandgap would be highly desirable because it would allow great flexibility in design and optimization of such devices, in particular if it could be tuned by applying a variable external electric field. However, in conventional materials, the bandgap is fixed by their crystalline structure, preventing such bandgap control. Here we demonstrate the realization of a widely tunable electronic bandgap in electrically gated bilayer graphene. Using a dual-gate bilayer graphene field-effect transistor (FET)[2] and infrared microspectroscopy[3–5], we demonstrate a gate-controlled, continuously tunable bandgap of up to 250 meV. Our technique avoids uncontrolled chemical doping[6–8] and provides direct evidence of a widely tunable bandgap—spanning a spectral range from zero to mid-infrared—that has eluded previous attempts[2,9]. Combined with the remarkable electrical transport properties of such systems, this electrostatic bandgap control suggests novel nanoelectronic and nanophotonic device applications based on graphene.

Graphene's unique electronic band structure has led to fascinating phenomena, exemplified by massless Dirac fermion physics[10–12] and an anomalous quantum Hall effect[13–16]. With one more graphene layer added, bilayer graphene has an entirely different (and equally interesting) band structure. Most notably, the inversion symmetric AB-stacked bilayer graphene is a zero-bandgap semiconductor in its pristine form. But a non-zero bandgap can be induced by breaking the inversion symmetry of the two layers. Indeed, a bandgap has been observed in a one-side chemically doped epitaxial graphene bilayer[6,8].

Of particular importance, however, is the potential of a continuously tunable bandgap through an electrical field applied perpendicularly to the sample[17–20]. Such control has proven elusive. Electrical transport measurements on gated bilayer exhibit insulating behaviour only at temperatures below 1 kelvin[2], suggesting a bandgap value much lower than theoretical predictions[17,18]. Optical studies of bilayers have so far been limited to samples with a single electrical gate[4,5,9], in which carrier doping effects dominate and obscure the signatures of a gate-induced bandgap. Such lack of experimental evidence has cast doubt on the possibility of achieving gate-controlled bandgaps in graphene bilayers[9].

Here, we use novel dual-gate graphene FETs to demonstrate unambiguously a widely field-tunable bandgap in bilayer graphene with infared absorption spectroscopy. By using both top and bottom gates in the graphene FET device we are able to control independently the two key semiconductor parameters: electronic bandgap and carrier doping concentration.

The electronic structure near the Fermi level of an AB-stacked graphene bilayer features two nearly parallel conduction bands above two nearly parallel valence bands (Fig. 1d)[21]. In the absence of gating, the lowest conduction band and highest valence band touch each other with a zero bandgap. Upon electrical gating, the top and bottom electrical displacement fields D_t and D_b (Fig. 1c) produce two effects (Fig. 1d): The difference of the two, $\delta D = D_b - D_t$, leads to a net carrier doping, that is, a shift of the Fermi energy (E_F). The average of the two, $\bar{D} = (D_b + D_t)/2$, breaks the inversion symmetry of the bilayer and generates a non-zero bandgap D[7,17,18]. By setting δD to zero and varying $\bar{D}$, we can tune the bandgap while keeping the bilayer charge neutral. Sets of D_b and D_t leading to $\delta D = 0$ define the bilayer 'charge neutral points' (CNPs). By varying δD above or below zero, we can inject electrons or holes into the bilayer and shift the Fermi level without changing the bandgap. In our experiment the drain electrode is grounded and the displacement fields D_t and D_b are tuned independently by top and bottom gate voltages (V_t and V_b) through the relations $D_b = +\varepsilon_b(V_b - V_b^0)/d_b$ and $D_t = -\varepsilon_t(V_t - V_t^0)/d_t$. Here ε and d are the dielectric constant and thickness of the dielectric layer and V^0 is the effective offset voltage due to initial environment-induced carrier doping.

The relationship between D and V for the top or bottom layers can be determined through electrical transport measurement[2]. Figure 1e shows the measured resistance along the graphene plane as a function of V_t with V_b fixed at different values, and CNPs can be identified by the peaks in the resistance curves, because charge neutrality results in a maximum resistance. The deduced CNPs, in terms of (V_t, V_b), are plotted in Fig. 1f. V_t and V_b are linearly related with a slope of about 0.15, consistent with the expected value of $-(\varepsilon_b d_t)/(\varepsilon_t d_b)$, where $d_b = 285$ nm, $\varepsilon_b = 3.9$ for thermal SiO_2, and $d_t = 80$ nm, $\varepsilon_t = 7.5$ for amorphous Al_2O_3. The peak resistance differs at different CNPs (Fig. 1e) because the field-induced bandgap itself differs. Lower peak resistance comes from a smaller bandgap. Thus, the lowest peak resistance allows us roughly to identify the zero-bandgap CNP ($D_b = D_t = 0$) and determine the offset top and bottom gate voltages from environment doping to be $V_t^0 \approx -5$ V and $V_b^0 \approx 10$ V. With the values of ε/d and gate voltage offsets, the displacement electric field can be determined within an uncertainty of about 10%. We note that although CNP resistance data shows an increase with the field-induced bandgap, the increase is much smaller than expected for a large energy gap opening. This is attributed to extrinsic conduction through defects and carrier doping from charge impurities in our samples.

To determine the true bilayer bandgap reliably, we used infrared microspectroscopy[3,4]. Such an optical determination of the electronic

[1]Department of Physics, University of California at Berkeley, [2]Advanced Light Source Division, Lawrence Berkeley National Laboratory, [3]Materials Science Division, Lawrence Berkeley National Laboratory, [4]Earth Sciences Division, Lawrence Berkeley National Laboratory, Berkeley, California 94720, USA. †Present address: Department of Photonics and Institute of Electro-optical Engineering, National Chiao Tung University, Hsinchu, Taiwan 30010.
*These authors contributed equally to this work.

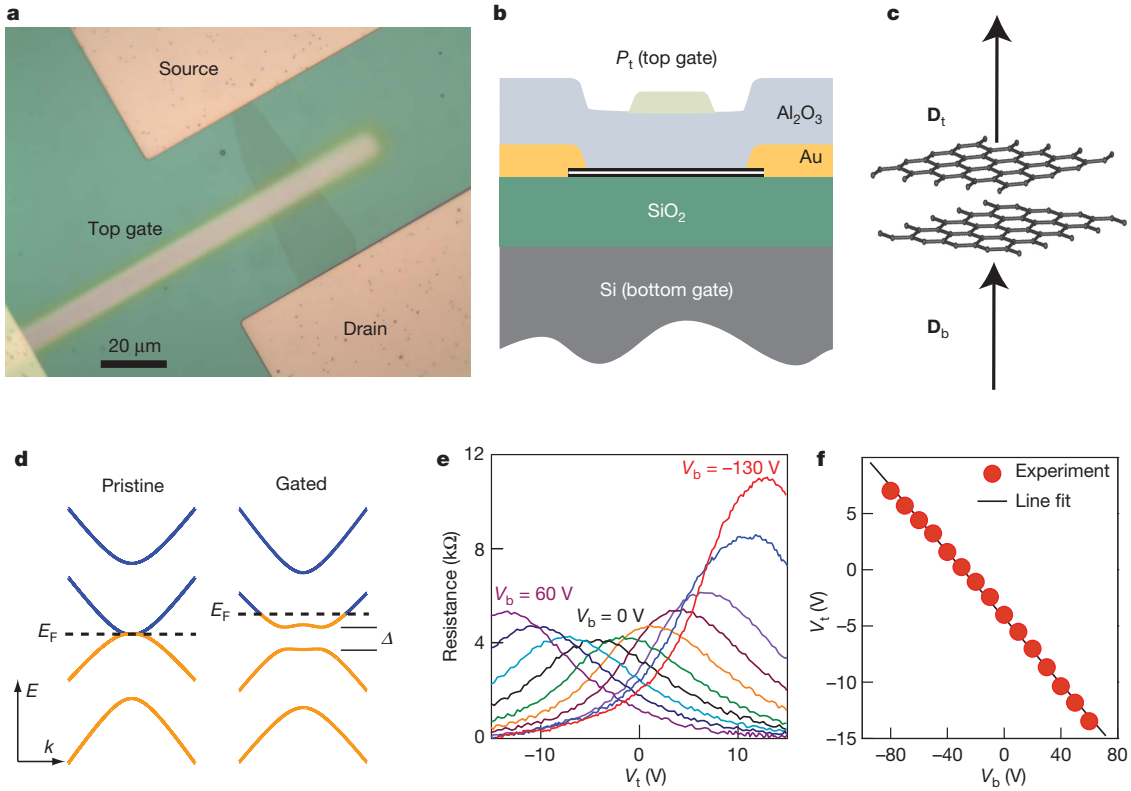

Figure 1 | Dual-gated bilayer graphene. **a**, Optical microscopy image of the bilayer device (top view). **b**, Illustration of a cross-sectional side view of the gated device. **c**, Sketch showing how gating of the bilayer induces top (D_t) and bottom (D_b) electrical displacement fields. **d**, Left, the electronic structure of a pristine bilayer has zero bandgap. (k denotes the wavevector.) Right, upon gating, the displacement fields induces a non-zero bandgap Δ and a shift of the Fermi energy E_F. **e**, Graphene electrical resistance as a function of top gate voltage V_t at different fixed bottom gate voltages V_b. The traces are taken with 20 V steps in V_b from 60 V to −100 V and at $V_b = -130$ V. The resistance peak in each curve corresponds to the CNP ($\delta D = 0$) for a given V_b. **f**, The linear relation between top and bottom gate voltages that results in bilayer CNPs.

bandgap is generally less affected by defects or doping than electrical transport measurements[2]. Figure 2b shows the gate-induced bilayer absorption spectra at CNPs ($\delta D = 0$) with $\bar{D} = 1.0\,\mathrm{V\,nm^{-1}}$, $1.4\,\mathrm{V\,nm^{-1}}$, $1.9\,\mathrm{V\,nm^{-1}}$ and $3.0\,\mathrm{V\,nm^{-1}}$. The absorption spectrum of the sample at the zero-bandgap CNP ($\bar{D} = 0$) has been subtracted as a background reference to eliminate contributions to the absorption from the substrate and gate materials. Two distinct features are present in the spectra, a gate-dependent peak below 300 meV and a dip centred around 400 meV. These arise from different optical transitions between the bilayer electronic bands, as illustrated in Fig. 2a. Transition I is the tunable bandgap transition that accounts for the gate-induced spectral response at energies lower than 300 meV. Transitions II, III, IV and V

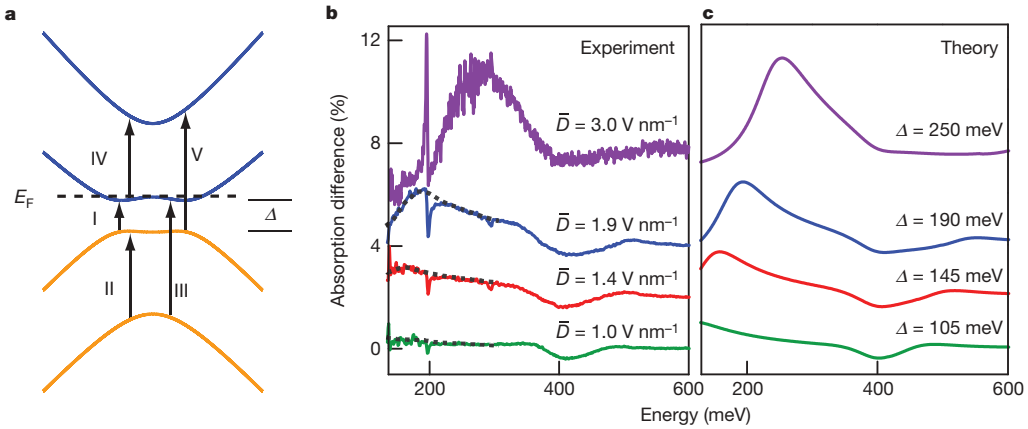

Figure 2 | Bilayer energy gap opening at strong electrical gating. **a**, Allowed optical transitions between different sub-bands of a graphene bilayer. Curves are offset from zero for clarity. **b**, Gate-induced absorption spectra at CNP for different applied displacement fields $\bar{D}$ (with the spectrum for zero-bandgap CNP subtracted as reference). For clarity the upper traces were displaced by 2%, 4% and 8%, respectively. Absorption peaks due to transition I at gate-induced bandgaps are apparent (dashed black lines are guides to the eye). At the same time, a reduction of absorption below the bandgap is expected. This reduction is clearly observed in the trace with the largest bandgap ($\Delta = 250$ meV) in our experimental spectral range. The sharp asymmetric resonance observed near 200 meV is due to Fano resonance of the zone-centre G-mode phonon with the continuum electronic transitions. The broad feature around 400 meV is due to electronic transitions II, III, IV and V. **c**, Theoretical prediction of the gate-induced absorption spectra based on a tight-binding model where the bandgap value is taken as an adjustable parameter. The fit provides an accurate determination of the gate-tunable bandgap at strong electrical gating.

occur at and above the energy of parallel band separation ($\gamma \equiv 400$ meV) and contribute to the spectral feature near 400 meV.

The absorption peak below 300 meV in Fig. 2b shows pronounced gate tunability: it gets stronger and shifts to higher energy with increasing $\bar{D}$. This arises because as the bandgap increases, so does the density of states at the band edge. The peak position, corresponding to the bandgap, increases from 150 meV at $\bar{D} = 1.4\ \mathrm{V\,nm^{-1}}$ to 250 meV at $\bar{D} = 3\ \mathrm{V\,nm^{-1}}$. This shows directly that the bandgap can be continuously tuned up to at least 250 meV by electrical gating. The bandgap transitions are remarkably strong: optical absorption can reach 5% in two atom layers, corresponding to an oscillator strength that is among the highest of all known materials. On the basis of the sum rule, a reduction of absorption below the bandgap should accompany the prominent band-edge absorption peak. This absorption reduction is clearly observed in the trace with the largest bandgap ($\Delta = 250$ meV) in our experimental spectral range. We also notice in Fig. 2b a very sharp spectral feature at 1,585 $\mathrm{cm^{-1}}$ (about 200 meV). This narrow resonance can be attributed to the zone-centre G-mode phonon in graphene[22]. The asymmetric lineshape originates from Fano interference between the discrete phonon and continuous electronic (bandgap) transitions.

When the displacement field $\bar{D}$ is weak ($<1.2\ \mathrm{V\,nm^{-1}}$), the gate-induced bandgap becomes too small to be measured directly. However, it can still be extracted from spectral changes around 400 meV induced by electron doping through gating. This is achieved by measuring the difference in bilayer absorption for $\delta D = 0$ (CNP) and $\delta D = 0.15\ \mathrm{V\,nm^{-1}}$ (electron-doped) at different fixed $\bar{D}$ values (Fig. 3a). We first examine the optical transitions in Fig. 2a, to understand the bilayer absorption difference due to electron doping. With electrons occupying the conduction band states, transition IV becomes stronger from extra filled initial states and transition III becomes weaker because of fewer available empty final states. However, transition IV is more prominent and gives rise to the observed peaks in the absorption difference spectra because all such transitions have similar energy owing to the nearly parallel conduction bands. When the bandgap increases with increasing $\bar{D}$, the lower conduction band moves up, but the upper conduction band hardly changes, making the separation between the two bands smaller. This will lead to a redshift of transition IV. Therefore, the shift of the peak in the difference spectrum can yield the bilayer bandgap when compared to theory. When the gate-induced bandgap is small, this shift equals roughly half of the bandgap energy. At higher $\bar{D}$ values, deviation from the near-parallel band picture becomes significant and a broadening of the absorption peak takes place (Supplementary Fig. S1).

We obtained quantitative understanding of the gate-induced bandgap and its associated optical properties through comparison of our data to theoretical predictions. We modelled the bilayer absorption using the self-consistent tight-binding model following ref. 23, except that the bandgap was treated as a fitting parameter here. We have included a room-temperature thermal broadening of 25 meV and an extra inhomogeneous broadening of 60 meV to account for sample inhomogeneity. We note that this large inhomogeneous broadening is comparable to that estimated from transport studies[24] and it accounts for the difficulty in electrical determination of the bilayer graphene bandgap. Figure 2c shows our calculated gate-induced absorption spectra and bandgaps of bilayer graphene extracted by matching the absorption peak between 130–300 meV in the 'large bandgap' regime ($\Delta > 120$ meV). Agreement with the experimental spectra (Fig. 2b) is excellent, except for the phonon contribution at ~200 meV, which is not included in our model. For the 'small bandgap' regime ($\Delta < 120$ meV), we are able to determine the bilayer bandgap by comparing our model calculations to the measured absorption difference spectra shown in Fig. 3a. Our calculations (Fig. 3b) provide a good qualitative fit to the absorption peak that arises from electron transition IV: this absorption peak shifts to lower energy as the bandgap becomes larger, reproducing the observed behaviour at increasing displacement field $\bar{D}$ in Fig. 3a. By matching the experimental and theoretical values of this absorption peak shift, we can extract the bilayer bandgap at different $\bar{D}$ in the 'small bandgap' regime.

Figure 4 shows a plot of the experimentally derived gate-tunable bilayer bandgap over the entire range ($0 < \Delta < 250$ meV) as a function of applied displacement field $\bar{D}$ (data points). Our experimental bandgap results are compared to predictions based on self-consistent tight-binding calculations (black trace)[23], *ab initio* density functional (red trace)[18], and unscreened tight-binding calculations (dashed blue line)[7]. Clearly the inclusion of graphene self-screening is crucial in achieving good agreement with the experimental data, as in the self-consistent tight-binding and *ab initio* calculations. The *ab initio*

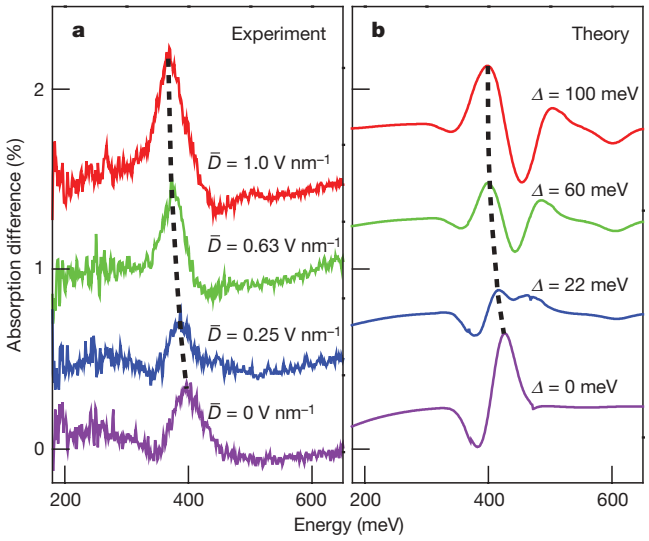

Figure 3 | Bilayer energy gap opening at weak electrical gating. **a**, Absorption difference between electron-doped ($\delta D = 0.15\ \mathrm{V\,nm^{-1}}$) and charge-neutral bilayers ($\delta D = 0$) at different average displacement fields $\bar{D}$. The curves are displaced by multiples of 0.5% for clarity. The absorption peak is mainly due to increased absorption between nearly parallel conduction bands from extra filled initial states (transition IV in Fig. 2a). This absorption peak shifts to lower energy due to the opening of the bilayer bandgap with increasing $\bar{D}$. **b**, Calculated absorption difference spectra based on a tight-binding model using the gate-induced bandgap as an adjustable parameter. Good agreement between theory and experiment on the absorption peak redshift (black dashed lines in **a** and **b**) yields the gate-induced bilayer bandgap at weak gating.

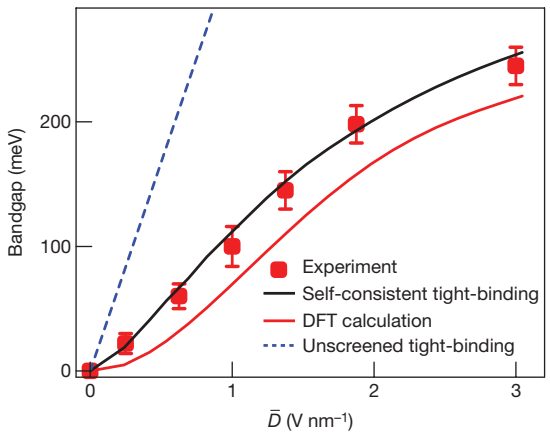

Figure 4 | Electric-field dependence of tunable energy bandgap in graphene bilayer. Experimental data (red squares) are compared to theoretical predictions based on self-consistent tight-binding (black trace), *ab initio* density functional (red trace), and unscreened tight-binding calculations (blue dashed trace). The error bar is estimated from the uncertainty in determining the absorption peaks in the spectra.

calculation predicts a slightly smaller bandgap than does the tight-binding model. This is partly owing to the different values used for onsite interlayer coupling γ_1, which is 0.4 eV for the tight binding and 0.34 eV for the *ab initio* calculations. Similar underestimation of bandgaps by *ab initio* local density functional calculations is common for semiconductors[25].

Our study shows a confluence of interesting electronic and optical properties in graphene bilayer FETs, which provide appealing opportunities for new scientific exploration and technological innovation. The achieved gate-tunable bandgap (250 meV), an order of magnitude higher than the room-temperature thermal energy (25 meV), emphasizes the intrinsic potential of bilayer graphene for nanoelectronics. With the tunable bandgap reaching the infrared range, and with the unusually strong oscillator strength for the bandgap transitions, bilayer graphene may enable novel nanophotonic devices for infrared light generation, amplification and detection.

METHODS SUMMARY

Graphene bilayer flakes were exfoliated from graphite and deposited onto Si/SiO_2 wafers as described in ref. 26. Bilayers were identified by optical contrast in a microscope and subsequently confirmed via Raman spectroscopy[22]. Source and drain electrodes (Au, thickness 30 nm) for transport measurement were deposited directly onto the graphene bilayer through a stencil mask under vacuum. The doped Si substrate under a 285-nm-thick SiO_2 layer was used as the bottom gate. The top gate was formed by sequential deposition of an 80-nm-thick Al_2O_3 film and a sputtered strip of 20-nm-thick Pt film. The Pt electrode was electrically conductive and optically semi-transparent. Two-terminal electrical measurements were used for transport characterization. We extracted a carrier mobility of $\sim$1,000 $cm^2 V^{-1} s^{-1}$ from the electrical transport measurements. Infrared transmission spectra of the dual-gated bilayer were obtained using the synchrotron infrared beamline at the Advanced Light Source at Berkeley and a microFourier transform infrared spectrometer. All measurements were performed at room temperature (293 K).

Received 26 February; accepted 30 April 2009.

1. Sze, S. M. & Ng, K. K. *Physics of Semiconductor Devices* (Wiley-Interscience, 2006).
2. Oostinga, J. B., Heersche, H. B., Liu, X. L., Morpurgo, A. F. & Vandersypen, L. M. K. Gate-induced insulating state in bilayer graphene devices. *Nature Mater.* **7,** 151–157 (2008).
3. Li, Z. Q. *et al.* Dirac charge dynamics in graphene by infrared spectroscopy. *Nature Phys.* **4,** 532–535 (2008).
4. Wang, F. *et al.* Gate-variable optical transitions in graphene. *Science* **320,** 206–209 (2008).
5. Li, Z. Q. *et al.* Band structure asymmetry of bilayer graphene revealed by infrared spectroscopy. *Phys. Rev. Lett.* **102,** 037403 (2009).
6. Ohta, T., Bostwick, A., Seyller, T., Horn, K. & Rotenberg, E. Controlling the electronic structure of bilayer graphene. *Science* **313,** 951–954 (2006).
7. Castro, E. V. *et al.* Biased bilayer graphene: semiconductor with a gap tunable by the electric field effect. *Phys. Rev. Lett.* **99,** 216802 (2007).
8. Zhou, S. Y. *et al.* Substrate-induced bandgap opening in epitaxial graphene. *Nature Mater.* **6,** 770–775 (2007).
9. Kuzmenko, A. B. *et al.* Infrared spectroscopy of electronic bands in bilayer graphene. Preprint at <http://arxiv.org/abs/0810.2400> (2008).
10. Geim, A. K. & Novoselov, K. S. The rise of graphene. *Nature Mater.* **6,** 183–191 (2007).
11. Katsnelson, M. I., Novoselov, K. S. & Geim, A. K. Chiral tunnelling and the Klein paradox in graphene. *Nature Phys.* **2,** 620–625 (2006).
12. Huard, B. *et al.* Transport measurements across a tunable potential barrier in graphene. *Phys. Rev. Lett.* **98,** 236803 (2007).
13. Novoselov, K. S. *et al.* Two-dimensional gas of massless Dirac fermions in graphene. *Nature* **438,** 197–200 (2005).
14. Zhang, Y. B., Tan, Y. W., Stormer, H. L. & Kim, P. Experimental observation of the quantum Hall effect and Berry's phase in graphene. *Nature* **438,** 201–204 (2005).
15. Novoselov, K. S. *et al.* Unconventional quantum Hall effect and Berry's phase of 2 pi in bilayer graphene. *Nature Phys.* **2,** 177–180 (2006).
16. McCann, E. & Fal'ko, V. I. Landau-level degeneracy and quantum hall effect in a graphite bilayer. *Phys. Rev. Lett.* **96,** 086805 (2006).
17. McCann, E. Asymmetry gap in the electronic band structure of bilayer graphene. *Phys. Rev. B* **74,** 161403 (2006).
18. Min, H. K., Sahu, B., Banerjee, S. K. & MacDonald, A. H. Ab initio theory of gate induced gaps in graphene bilayers. *Phys. Rev. B* **75,** 155115 (2007).
19. Lu, C. L., Chang, C. P., Huang, Y. C., Chen, R. B. & Lin, M. L. Influence of an electric field on the optical properties of few-layer graphene with AB stacking. *Phys. Rev. B* **73,** 144427 (2006).
20. Guinea, F., Neto, A. H. C. & Peres, N. M. R. Electronic states and Landau levels in graphene stacks. *Phys. Rev. B* **73,** 245426 (2006).
21. Abergel, D. S. L. & Fal'ko, V. I. Optical and magneto-optical far-infrared properties of bilayer graphene. *Phys. Rev. B* **75,** 155430 (2007).
22. Ferrari, A. C. *et al.* Raman spectrum of graphene and graphene layers. *Phys. Rev. Lett.* **97,** 187401 (2006).
23. Zhang, L. M. *et al.* Determination of the electronic structure of bilayer graphene from infrared spectroscopy. *Phys. Rev. B* **78,** 235408 (2008).
24. Adam, S. & Sarma, S. D. Boltzmann transport and residual conductivity in bilayer graphene. *Phys. Rev. B* **77,** 115436 (2007).
25. Hybertsen, M. S. & Louie, S. G. Electron correlation in semiconductors and insulators—band-gaps and quasi-particle energies. *Phys. Rev. B* **34,** 5390–5413 (1986).
26. Novoselov, K. S. *et al.* Two-dimensional atomic crystals. *Proc. Natl Acad. Sci. USA* **102,** 10451–10453 (2005).

Supplementary Information is linked to the online version of the paper at www.nature.com/nature.

Acknowledgements This work was supported by the Office of Basic Energy Sciences, US Department of Energy under contract DE-AC03-76SF0098 (Materials Science Division) and contract DE-AC02-05CH11231 (Advanced Light Source). F.W., Y.Z. and T.-T.T. acknowledge support from a Sloan fellowship, a Miller fellowship and a fellowship from the National Science Council of Taiwan, respectively.

Author Information Reprints and permissions information is available at www.nature.com/reprints. The authors declare no competing financial interests. Correspondence and requests for materials should be addressed to F.W. (fengwang76@berkeley.edu).